Carbon 169 (2020) 248–257

Contents lists available at ScienceDirect

Carbon

journal homepage: www.elsevier.com/locate/carbon

Ultrastrong adhesion of fluorinated graphene on a substrate: *In situ* electrochemical conversion to ionic-covalent bonding at the interface

Yu-Yu Sin [a], Cheng-Chun Huang [a], Cin-Nan Lin [b], Jui-Kung Chih [b], Yu-Ling Hsieh [b], I-Yu Tsao [c], Ju Li [d], Ching-Yuan Su [a, b, *]

[a] Graduate Institute of Energy Engineering, National Central University, Tao-Yuan, 32001, Taiwan
[b] Department of Mechanical Engineering, National Central University, Tao-Yuan, 32001, Taiwan
[c] Institute of Materials Science and Engineering, National Central University, Tao-Yuan, 32001, Taiwan
[d] Department of Nuclear Science and Engineering and Department of Materials Science and Engineering, Massachusetts Institute of Technology, Cambridge, MA, 02139, USA

ARTICLE INFO

Article history:
Received 20 May 2020
Received in revised form
10 July 2020
Accepted 28 July 2020
Available online 1 August 2020

Keywords:
Fluorination-graphene
Electrophoresis
Strong graphene film
Copper fluoride

ABSTRACT

Graphene shows unique properties such as high mechanical strength and high thermal and chemical stability, making it promising for versatile applications. However, the lack of either interlayer or interface covalent bonds causes this type of 2D materials assembled via van der Waals forces to suffer from weak adhesion with the underlying substrates, thus hindering their application. In this study, a novel method based on a hydrothermal reaction was proposed to synthesize fluorinated graphene (FG) through a facile, scalable, and highly safe process, where a mixture of poly(perfluorosulfonic acid) ($C_7HF_{13}O_5S \cdot C_2F_4$, PFSA) and graphene oxide (GO) as the precursor was employed. The FG sheets prepared by the electrophoretic deposition (EPD) method exhibit superior conformity layered structure on a metal foil. Due to the in situ formation of ionic-covalently bonded F—Cu—F and Cu—F—C between fluorine on the FG sheets and dissolved Cu ions from the copper foil, the deposited film shows ultrastrong adhesion that can sustain up to 3 MPa of shear force. Furthermore, by changing the parameters in the EPD process, such as the EPD duration and applied voltage, the thickness and hydrophobicity of the film can be well controlled from 0.20 μm to 2.51 μm with a contact angle from 93.03° to 122.44°. This study provides a new strategy to prepare a robust film for the assembly of 2D materials, not limited to graphene, with ultrastrong adhesion on substrates, which could solve the long-reported issue of weak adhesion and low durability of graphene-/2D-based functional composites and coatings.

1. Introduction

Graphene, a 2D van der Waals atomic material, shows unique material properties, such as high mechanical strength, thermal conductivity, and chemical stability, making it promising for versatile applications. In particular, the surface modification of graphene on a variety of substrates introduces new functional properties. For instance, surface modification creates advanced functional properties, such as hydrophobic modification, allowing the modified graphene to be applied in self-cleaning, ice repelling, and increasing the heat transfer efficiency of thermal technologies [1–3]. Currently used hydrophobic modification processes, such as coating hydrophobic polymers and machining surface microstructures, are used to increase the hydrophobicity of the workpiece surface; however, hydrophobic polymers always show poor stability during long-term operation, and the machining process of the microstructure shows higher costs and is limited by the complex shape of the substrate [4–6]. Therefore, the development of an effective approach for hydrophobic modification with reliable materials and a cost-effective coating process while enabling operation on versatile and complex surfaces is highly desired for practical applications.

Graphene exhibits the features of chemical stability and hydrophobicity, thus showing remarkable promise as a hydrophobic coating material [7]. Recently, several coating methods for preparing graphene films, such as chemical vapor deposition (CVD), the Langmuir-Blodgett (LB) method, and inkjet printing, have been

* Corresponding author. Graduate Institute of Energy Engineering, National Central University, Tao-Yuan, 32001, Taiwan.
E-mail address: cysu@ncu.edu.tw (C.-Y. Su).

https://doi.org/10.1016/j.carbon.2020.07.067
0008-6223/

proposed [8–10]. In the CVD method, the graphene on the metal substrate requires a high temperature process, thus altering the mechanical properties of the underlying substrate and limiting its applications. On the other hand, the other methods are either time-communing or limited to conformal coating on a complex substrate shape. Another long-term issue to be resolved is that these 2D material films lack strong interlayer or interface covalent bonds, causing them to suffer from low adhesion when coated on a substrate; thus, they are easily exfoliated by external forces, which hinders further applications [11,12]. Several methods have been proposed to address adhesion issues in 2D materials. A commonly used method is to add polymers such as poly(vinyl alcohol) (PVA) [13,14], poly(methyl methacrylate) (PMMA) [14], glutaraldehyde (GA) [15], and dopamine [16,17] as binders, forming crosslinks between the 2D materials to improve their mechanical properties; however, such additives improve only the mechanical properties while also considerably degrading other essential and unique properties of 2D materials. Liu et al. reported defect-facilitated crosslinking through an electrical Joule welding process to achieve a high joint strength up to 72 kPa between graphene layers. The solder-free welding method yielded a 3D structure via assembly of a 2D material without loss of the specific characteristics of the original material; however, the lack of adhesion between the 3D structure and the substrate was still unsolved, and the high temperature of up to 2800 °C during the process still limited the use of this method in practical applications [18]. Another method reported by Xu et al. involved predepositing a layer of chromium to bond with graphene, forming a $Cr_{23}C_6$ buffer layer, thus strongly and more uniformly anchoring the graphene film on the underlying substrate compared to direct coating on mild steel. This method provided a new route for coating a 2D material on a metal substrate, resulting in greater adhesion and improved uniformity. However, the process was too complicated, and the surface material still lacked strong bonding, thus still suffering from a high risk of being peeled off and consequently degrading the properties of the coating [19].

On the other hand, a method to form the 3D structure from 2D materials by converting weak van der Waals forces into strong covalent bonding has been proposed. For example, Sreepal et al. proposed the transfer of InSe into Se-doped InF_3 by fluorination to convert the interaction between each layer from weak van der Waals forces to covalent bonding [20]. Some theoretical studies have also demonstrated the conversion of multilayer graphene into an ultrathin diamond structure by attaching atoms (fluorine, hydrogen) or hydroxyl groups onto the surface of graphene [21–25]. However, currently, synthesis by this route suffers from either the requirement of high pressure or the limitation of a small domain (bilayer) of such a covalent bonding structure [26–28]. This new concept of converting the bonding between different layers from weak van der Waals forces into strong covalent bonds can provide new inspiration to develop a 3D structure from 2D materials, leading to better applications on functional nanocomposites and thin films.

For the application of uniform graphene or 2D films on substrates, unlike other methods, such as spin/spray coating and injection printing, the current technique of electrophoretic deposition (EPD) is a colloidal process with the advantages of possible operation on complex substrate shapes, cost-effectiveness, simple equipment, low operating temperature, and high controllability of the deposited film by altering the electrical potential [29]. Graphene-based films synthesized by EPD have already been used in many applications, such as electromagnetic interference shielding [30], anti-reflective materials [31], and corrosion-resistant coatings [32,33].

Recently, graphene functionalized with fluorine, so-called fluorinated graphene (FG), was reported to alter the electronic and surface chemistry properties of graphene counterparts [34–36], and it exhibits a mechanical strength comparable to that of pristine graphene. Other unique properties, such as the extremely low surface friction coefficient, electrical insulation, and surface hydrophobic features, allow FG to be widely applied in functional coatings, nanoelectronics, and thermal technologies [37–41]. In particular, the film assembled by fluorinated graphene (FG) shows higher hydrophobicity than pristine graphene due to the existence of C–F bonds, thus resulting in an extremely lower surface free energy [42,43]. Moreover, FG was reported to stable up to 400 °C without degradation, suggesting higher durability, which is beneficial for practical usages. Typical methods to fabricate FG include (1) graphene treatment by exposure to XeF_2 gas [34,44]; (2) exfoliation of bulk fluorinated graphite [42,45,46]; and (3) hydrothermal treatment of GO by reactive agents such as HF and BF_3-etherate [47,48]. However, most of these methods employ toxic chemicals and dangerous procedures or result in low production yields, which hinders their scalable production and applications. Developing a safe, facile, scalable and eco-friendly process for preparing FG is still a challenge.

Herein, we developed a novel method to prepare FG by a hydrothermal process with the addition of poly(perfluorosulfonic acid) ($C_7HF_{13}O_5S \cdot C_2F_4$, PFSA) as a precursor in the GO solution. A robust hydrophobic film with FG was deposited by electrophoretic deposition (EPD) on the copper substrate. Tensile testing demonstrated that the FG film was successfully coated on the copper substrate with ultrastrong adhesion and could sustain 3 MPa of shear force, which, to the best of our knowledge, is the best value reported for the adhesion force of graphene and other 2D materials on a substrate. The extremely high adhesion was caused by the in situ formation of ionic-covalently bonded F–Cu–F and Cu–F–C between fluorine on the FG sheets and dissolved Cu ions from the copper foil during the EPD process. The mechanism of formation of this strong bonding state was investigated in detail through X-ray photoelectron spectroscopy (XPS) and high-resolution transmission electron microscopy (HRTEM) characterizations. Moreover, by using different EPD parameters, such as applied voltage and EPD duration, the thickness and hydrophobicity could be well controlled from 0.20 μm to 2.51 μm with a contact angle from 93.03° to 122.44°. With the high controllability and high adhesion of the deposited film, this FG film deposited by EPD provides a new pathway for facile and robust (thermal stability up to 300 °C) hydrophobic surface modification. This work describes a new method to scalably produce FG and new results on the ultrastrong adhesion of graphene to a metal substrate, which could open a new avenue for resolving the long-existing issue of weak adhesion and low durability on the practical applications of graphene-based functional coating films.

2. Experimental section

2.1. Synthesis of fluorinated graphene

Graphene oxide (GO) in aqueous solution (1.30 mL) with a concentration of 7.72 mg/mL was first synthesized by the improved Hummer's method described in our previous works [49,50]. Subsequently, 6 mL of a mixture of 5–6 wt % poly (perfluorosulfonic acid) ($C_7HF_{13}O_5S \cdot C_2F_4$, CAS Number: 31175-20-9) in 1-propanol (42–54 wt%), water (40–50 wt%) and ethyl alcohol (<8 wt%) was mixed with 4 mL of dimethylformamide (DMF) in GO solutions with electromagnetic stirring and ultrasonic vibration for 10 min. The fluorination reaction proceeded by the hydrothermal method, where the as-prepared mixture solution was poured into an autoclave and heated at 200 °C for 15 h to obtain fluorinated graphene

(FG). To extract the pure FG sheets from the mixture, centrifugation was employed at 9000 rpm for 60 min to remove the waste liquid. After that, the aggregated FG flakes were washed with acetone by ultrasonication for 10 min and centrifuged at 9000 rpm for 30 min. Finally, the obtained FG sheets were dispersed in ethanol (0.2 mg/mL) as a suspension for subsequent use.

2.2. FG film prepared by the electrophoretic deposition (EPD) method

Copper foil (Alfa Aesar, No. 13382, thickness 25 μm, purity 99.8%) was selected as the deposition substrate and immersed in the FG dispersion. Before the EPD process, isopropanol (IPA) was used to wipe the surface of copper foil with tissue to remove dust and oils. To avoid the effect of the initial surface roughness of copper foil, when analyzing the thickness and surface roughness of deposited FG film by EDP a 400 nm thick Cu was sputtered on a silicon substrate, from which the surface roughness was about 16 nm. FG sheets were deposited onto the copper foil through the electrophoretic deposition (EPD) method, and a Cu foil with an identical area was prepared as counter electrode in parallel at a distance of 5 mm; the applied voltage ranged from 10 V to 50 V for 30 s to 10 min by a DC power supply (MOTECH, PPS-2018A). Due to the negative charge of FG sheets in ethanol, the FG sheets were deposited on the anode. After the EPD process, the specimens were dried in air at room temperature for over 1 day to remove residual solvent from the deposited FG film.

2.3. Characterization

The morphology of the FG sheets and the deposited FG film were investigated by scanning electron microscopy (SEM, JEOL JSM-7000F) at 10 kV. The thickness profiles of the GO and FG sheets were recorded by atomic force microscopy (AFM, NT-MDT SOLVER Nano), and the crystallinities were characterized by Raman spectroscopy (Horiba HR-550) with a single-laser excitation wavelength of 532 nm and a laser spot size of 1 μm. The chemical identity was determined by X-ray photoelectron spectroscopy (XPS, Thermo VG-Scientific Sigma Probe) with monochromatic Al-Kα X-ray radiation (1486.6 eV). The cross-sectional specimens were prepared by using a dual-beam focused-ion beam (FIB, FEI VERSA 3D) and investigated by low-vacuum SEM (LV-SEM, HITACHI S−3500 N). The high-resolution transmission electron microscopy (HRTEM) and the selected area electron diffraction (SAED) of the deposited FG film were performed by means of a JEOL-2100 instrument operated at 200 kV. The thickness of the deposited FG film was measured by a surface profiler (BRUKER DektakXT). The hydrophobicity was characterized by a contact angle analyzer (CA-XP150). The surface roughness was measured by a surface roughness analyzer (ACCRETECH SURCOM 130A) with a 2 μm diameter probe (ACCRETECH KP66 DM43801). The analysis of adhesion for the deposited FG film was carried out by tensile testing (Hung Ta HT-9102), and the peel-off interface SEM images were obtained by JEOL and JSM-7610F operated at 15 kV.

3. Results and discussion

In this study, we develop a novel method with safe and eco-friendly features to prepare fluorinated graphene efficiently through a simple hydrothermal route with a perfluorinated polymer. The fluorination procedure is illustrated in Fig. 1a, where graphene oxide (GO) was dispersed in dimethylformamide (DMF) as the starting material with the additive PFSA as the fluorinating agent (more detailed procedures are given in the experimental section). The synthesis temperature was 200 °C, where the PFSA was decomposed to give fluorine (F) radicals and other polymer fragments [51,52]. The oxygen groups of GO were found to efficiently decompose at this temperature and subsequently interact with the F radicals to form fluorinated graphene (FG). Note that the FG and byproduct (i.e., the polymer fragment) after the reaction was facilely separated since the polymer fragment was easily dissolved in the DMF solvent, followed by washing and removal after purification. As shown in the right panel of Fig. 1, FG could not be dispersed in water and suddenly aggregated on the solution surface, while it was temporarily dispersed in ethanol due to the hydrophobic nature of FG. Moreover, the color of the dispersion changed from brown to black after the fluorination reaction, indicating that the oxygen functional groups on GO were removed or replaced by fluorine atoms [53]. The concentration of PFSA in a DMF solution (from 20 to 70 vol %) was found to tailor the fluorination degree of FG, where the F/C ratio enabled tuning from 0.31 to 0.81 (see the XPS analysis in Fig. S1) and their corresponding contact angle (CA) with the water ranged from 97.34° to 112.28° (Fig. S2). The optimized F/C of 0.46, based on 60 vol % PFSA, enabled the most hydrophobic surface to be achieved (CA: 112.28°). Although higher loading of PFSA of up to 70 vol % led to a higher fluorination degree (F/C = 0.81), it was found that the CA was significantly decreased to 107.69°, possibly because the high viscosity of the PFSA/DMF solution hindered the fluorinated reaction and the unreacted PFSA fragment adsorbed on the FG surface, leading to a lower CA approaching the contact angle of the pure PFSA film (101.02°, as shown in Fig. S2). Fig. 1b–e shows the morphologies of GO and FG determined by scanning electron microscopy (SEM) and atomic force microscopy (AFM), indicating that the GO sheets were flattened on the substrate while the FG extended upwards, and a high density of wrinkles was clearly observed (Fig. 1c). The formation of highly winkled FG was attributed to the structural transformation from the sp^2 to sp^3 configuration and a lattice strain that induced high distortions of C–C bonds with carbon atoms out of the graphene basal plane (especially the CF and CF_3 specious) [35,54]. Fig. 1d and e shows the AFM profile of the GO and FG sheets. The thickness of the GO sheet was approximately 1.3 nm, suggesting one-to two-layered graphene. Moreover, the AFM profile revealed that FG shows a much higher surface roughness (Ra) of 0.35 nm than pristine GO sheets (0.08 nm), which was consistent with the SEM analysis results. Note that the zigzagged height profile in the FG sheet was observed (inset in Fig. 1e), which further confirm the highly wrinkled structure instead of the thickness of a single FG sheet.

Raman spectroscopy is an important tool for characterizing graphene-based materials. Fig. 1f shows the typical Raman spectra of GO and FG. The G peak (at ~1580 cm^{-1}) features the sp^2-hybridized C–C bond in graphene, while the D peak at 1350 cm^{-1} is indicative of lattice disorder, which is attributed to the high oxidation or fluorination on graphene [39]. Although GO and FG showed to be only one or two layers, the D band was relatively high (D/G ratio > 1) due to the high content of oxygen groups or fluorine atoms. Such high intensity of D band signal may inhibit 2D band thus 2D peak was missing in both GO and FG. This phenomenon was consistent with these reported works [39,49,55].

XPS was employed to characterize the bonding states of FG sheets, as shown in Fig. 1g. In addition to the bonding such as C–C (284.8 eV), C–O (286.4 eV), C=O (287.1 eV), and COO (288.8 eV) from the original GO, the deconvoluted C1s spectrum of the FG sheets shows several C–F bonding states, such as peaks attributed to C–F (288.2 eV), CF-CF_2 (289.9 eV), C–F_2 (292.1 eV), and C–F_3 (293.7 eV); moreover, the F1s peak of FG at 688.8 eV provides further evidence of the formation of C–F bonding states [56]. All of the above evidence indicated the success of the fluorination reaction by this method.

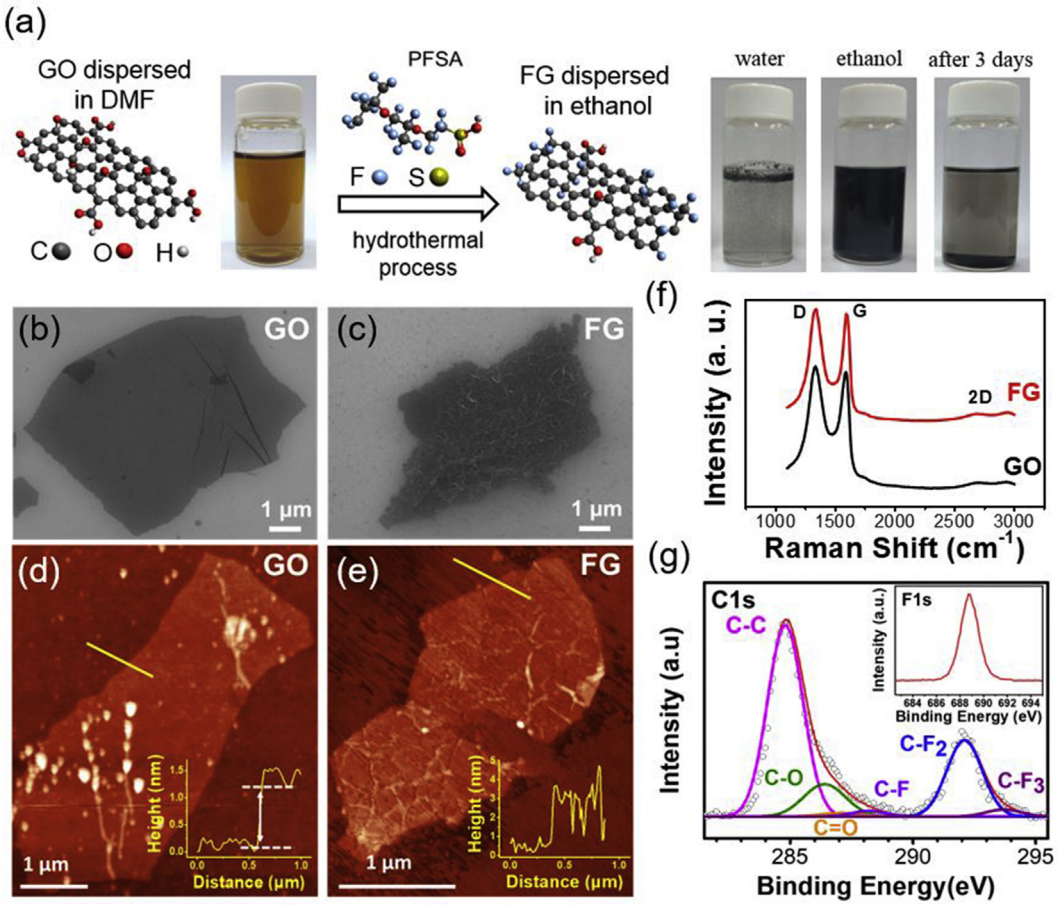

Fig. 1. (a) Schematic of the synthesis process of fluorinated graphene. (b) and (c) SEM images and (d) and (e) AFM images of GO and FG (the inset shows the height profile of the marked area). (f) Raman spectra of GO and FG. (g) The deconvoluted XPS spectrum of the C1s peak shows the C–O and C–F bonding states. The inset shows the F1s spectra at 688.8 eV. (A colour version of this figure can be viewed online.)

Due to the easy aggregation of FG when it was dispersed in ethanol, each EPD process was carried out after ultrasonication (10 min) to obtain a well-dispersed FG solution (detailed EPD procedure can be found in the experimental section). Fig. S3 shown the optical images on FG suspensions with a concentration ranged from 0.2 to 1.5 mg/mL and their corresponding FG films. The result indicates that the FG solution with a concentration higher than 0.2 mg/mL would serious aggregation to lower the uniformity of deposition film. On the other hand, the concentration lower than 0.2 mg/mL leads to a very lower deposition rate. Therefore the 0.2 mg/mL was chosen to be the optimal concentration in this report for obtaining a well-dispersed solution and high uniform film. The deposition was controlled by the applied voltage (10–50 V) and duration time (30 s–10 min). Fig. 2a shows the smooth and uniform FG film on the Cu substrate after deposition. The microstructure of the deposited films was characterized by SEM. For the case of 50 V for 30 s, a homogeneous thin-film assembly of the stacking FG sheets on Cu was observed (Fig. 2b); in particular, it was found that the deposited FG film conformally covered the roughed surface of Cu rolling marks, indicating that the EPD process enables superior coating on the micro-textured substrate. Note that after increasing the deposition duration to 10 min (Fig. 2c), the surface roughness increased accordingly, possibly due to deposition in a later period, and FG sheets accumulated in the suspension due to the poor dispersibility; thus, the crumpled FG sheets were directly transported to the Cu surface. The cross-section of the specimen formed at 50 V for 10 min was prepared by dual-beam focused-ion-beam (FIB), and Pt passivation was used to protect the FG film from the damage caused by the ion beam. The cross-sectional SEM image showed the layered structure of the FG sheets (Fig. 2d). The relation between the thickness of the film and the EPD duration is shown in Fig. 2e, where the film thickness increased with higher applied voltage and extended EPD duration. Note that the thickness obtained by this method can be well controlled from a few nanometers to a few micrometers, which is beneficial for feasible and broad applications. The slope of the correlated curve indicated the evolution of the deposition rate during this EPD process, from which higher rates of 12.5 nm/s (50 V) and 6.7 nm/s (10 V) were obtained before the first 3 min. After 3 min, the deposition rate tended to saturate and decreased to 3.3 and 1.4 nm/s due to the resistance of the predeposited FG film, which decreased the conductivity of the anode and screened the driving electrical field, thus hindering the deposition rate of the subsequent FG sheets [57,58]. According to these results, the FG film deposited by EPD showed film formation with diversity and high controllability of the film thickness.

The hydrophobicity of the films was defined by the CA measurement with DI water, and the results for all samples are shown in Fig. 3a. The CA was found to increase from 83.43° (pristine Cu) to 112.76° and 112.46° after EPD for 30 s by applying 10 V and 50 V, respectively. Before 3 min, the contact angle tended to continuously decrease with increasing EPD duration, which was attributed to the

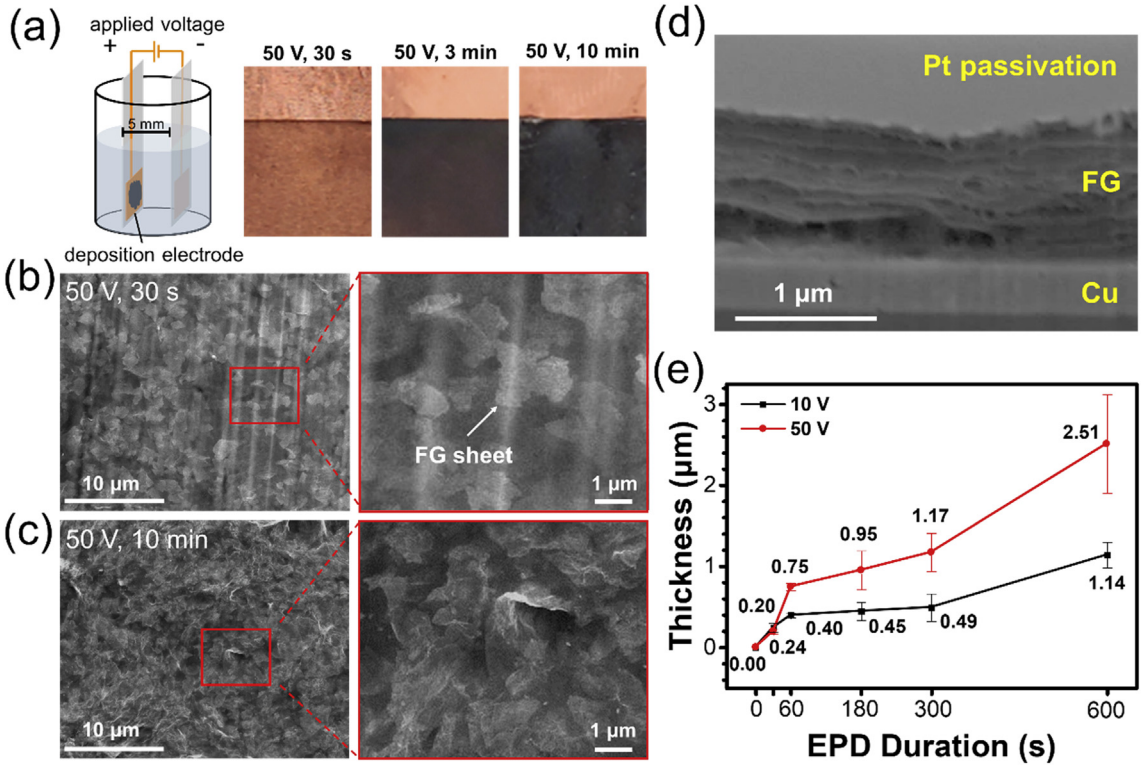

Fig. 2. (a) Schematic of the EPD process and optical images of FG films deposited on copper foil by applying 50 V for 30 s, 3 min, and 10 min. (b) and (c) SEM images of FG film surfaces synthesized at 50 V for 30 s and 10 min. (d) Cross-sectional SEM of the deposited FG film at 50 V for 10 min. (e) Relationship between thickness and EPD duration by applying different voltages. (A colour version of this figure can be viewed online.)

formation of a concentration gradient FG film, where the stacked FG sheets gradually decreased the fluorination degree from the bottom to the top surface, as evidenced by XPS analysis of the deposited FG film (Fig. 3c). The stoichiometry evolution of FG samples is shown in Fig. 3d. Additionally, the percentage of each bonding state (O- and F-related functional groups) for all samples with various EPD durations is shown in Table S1. It was found that the F-related bonding, including C—F, CF-CF_2, C—F_2, and C—F_3, tended to gradually decrease with increased EPD duration. In particular, the F/C ratio of the FG at the film surface gradually decreased until 3 min and then remained at approximately 22 at. % (Fig. 3d). The deposited FG film associated with the gradient fluorination degree of FG sheets was mainly attributed to the highly fluorinated FG, where the more negatively charged sheets migrated faster under the same electric field. This proposal was further evidenced by the zeta potential analysis (Fig. S4), where FG showed a higher surface charge (ζ_{mean} = −36.53 mV) than GO (ζ_{mean} = −32.67 mV) and exfoliated graphene (ζ_{mean} = −20.97 mV), indicating that the sheets exhibited more negative charges when the oxygen functional groups were replaced with fluorine atoms. Another interesting finding was that the CA (Fig. 3a) decreased to a minimum of 97.26° (10 V) and 93.03° (50 V) when the duration was 3 min; after this time, it increased above 120°, which was attributed to the increase in surface roughness, as evidenced in Fig. 3b, and was also consistent with the SEM morphology in Fig. 2c [59,60]. The surface roughness of bare Cu was initially 16 nm and then increased to 410 and 665 nm in association with increased duration; the roughened surface structure showed favorability to trap gas and thus promote the superhydrophobic FG film to 122.20°. To study the side effect of Cu corrosion during the EDP procedure, the Cu under the same EDP condition without coating materials was employed. The Ra of Cu substrate increase from 16 nm to 17 and 59 nm after 10min (Fig. S5a), which is much lower than the FG coated samples, indicating that the high surface roughness was mainly contributed from the FG coating. And the CA of these samples w/o FG were only slightly increased from 83.43° to 83.96° and 92.23° by the voltage of 10 or 50 V for 10 min (Fig. S5b). With these results, it is evidenced that the variations of CA and Ra were mainly dominated by the coating of FG film rather than the corrosion of Cu substrate. Thus, the FG film with EPD can be adjusted to form not only the surface but also the roughness-induced hydrophobicity by controlling the processing conditions.

Comparing to GO film prepared by the same EPD condition (applying 50 V for 10 min), It's clearly seen that only the edge parts of the FG film were peeled off by tape. On the other hand, GO film under the same testing condition was fully removed (Fig. S6). To study the adhesion between the FG film and the copper substrate, tensile testing was carried out on the samples as shown in Fig. 4a. Moreover, the scratch testing was employed (Fig. S7), where the loading force before reach 30 N, the film remained to be integrity while the film was partially detached when the force reached 30 N; thus the shear force of FG film could sustain at least up to 6.05 N. Also, even the force was increased to 50 N (Fig. S7c), part of the film could remain on the Cu substrate indicated that partial FG film could sustain a shear force over 11.5 N. The copper plate was coated with the FG film over an area of 1 cm^2 by EPD (50 V for 10 min), and then it was adhered to another copper plate by using a strong commercial glue (ethyl-2-cyanopropenoate). After that, a loading force was applied on the copper plate to peel off the FG film from the copper substrate, and the fracture interface is shown in the middle of Fig. 4a. The FG film can be totally removed, which indicates that the loading maximum corresponds to the adhesion

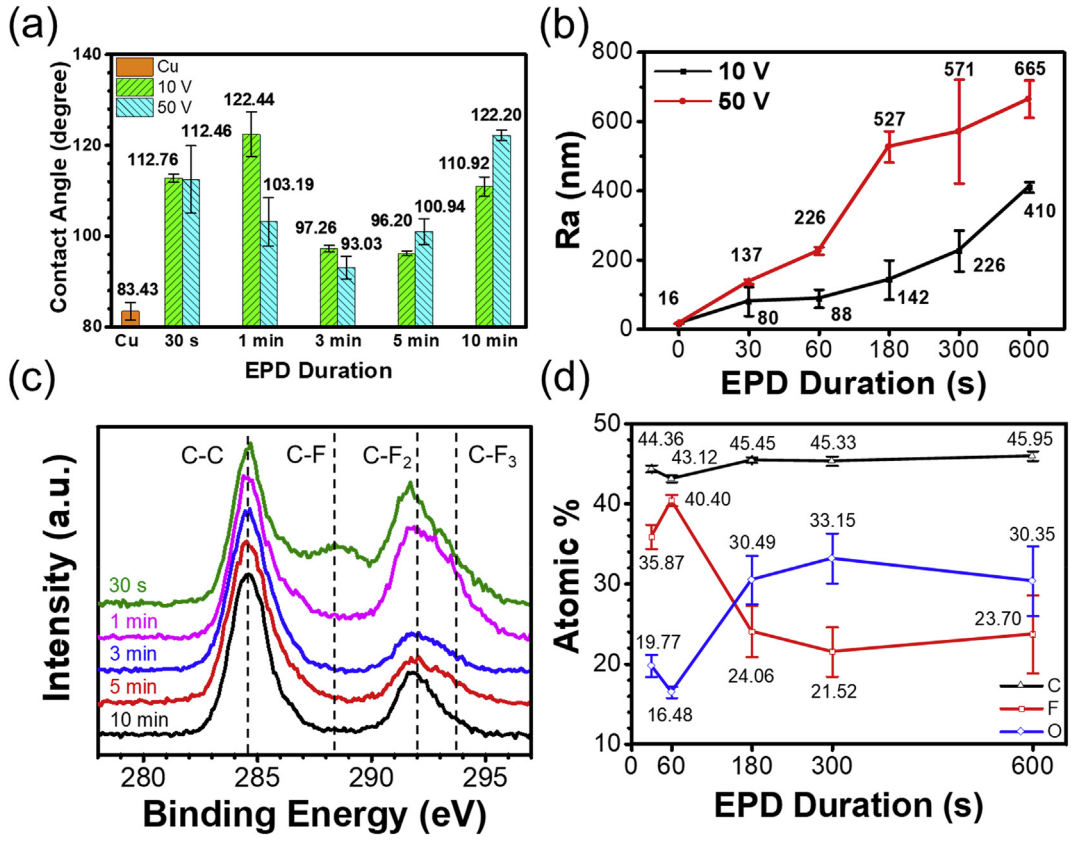

Fig. 3. (a) Contact angle of copper foil and FG films synthesized with different EPD durations and applied voltages. (b) Relationship between surface roughness (Ra) and EPD coating duration of FG films synthesized by different applied voltage. (c) XPS C1s spectra and (d) the elemental percentage of carbon, fluorine, and oxygen on the surface of FG films for the various coating duration conditions (at 50 V). (A colour version of this figure can be viewed online.)

between the FG film and the copper substrate. The SEM images of the fracture interface are shown in the right panel of Fig. 4a, where the FG sheets were found on both sides of the Cu plates, suggesting that the fracture occurred at the interface of the FG film and the Cu substrate; however, the adhesion between the partial FG sheets and the substrate was stronger than that between the FG sheets, thus leaving part of the sheets remaining on the Cu. In addition, the fracture loading was measured to be 300 N, indicating that the coated film can sustain the shear stress up to 3 MPa (Fig. 4b), to the best of our knowledge, is the recorded value among the reported adhesion force of graphene and other 2D materials on a substrate (Table S2). It was interesting to observe that the color of the copper substrate changed to light blue at the fractured interface, indicating the formation of unexpected interface materials during the EPD process. To characterize this interface material, HRTEM on the cross-sectional sample prepared by FIB was employed, and the corresponding selected area diffraction pattern (SADP) was acquired. From the SADP taken in region A, as indicated in Fig. 4c, the inverse distances of 8.227 nm^{-1} (segment a) and 4.934 nm^{-1} (segment b) allow us to elucidate the interface materials with lattice spacings of 0.161 nm and 0.203 nm corresponding to the X-ray diffraction (XRD) peaks at 57.34° and 44.68°, which were further assigned to CuF_2 (022) and (021), respectively [61]. From the HRTEM image of the middle region (B) of the sample, in which the CuF_2 particles were observed as well, the measured lattice spacing of 0.207 nm confirmed that the identical orientation of CuF_2 (021) was identical to that in region A. Furthermore, the feature peak at 684.8 eV observed in the XPS F1s spectrum (Fig. 4d) provided further evidence of the as-formed strong ionic bonding state of Cu–F_2.

According to the material analyses, we propose a model of the chemical reactions which were happened in the Cu anode during the EPD process as shown in Fig. 5. It was reported that once the graphene was dispersed in the organic solvent, charge transfer occurred between solvent and graphene [62]. In our case, the electrons were attracted to FG's surface due to the high donor number of ethanol, which made FG became negatively charged and thus moving toward anode under the applying electrical field. At the same time, Cu anode undergoes the corrosion and the estimated corrosion rate was 3.85 mm/year (the calculation detail is shown in Fig. S8) under applying 50 V, suggesting that about 72 nm of Cu corrosion during the 10 min of EPD process owing to the release of Cu^{2+} ions. As soon as FG sheets reached the copper surface, three possible pathways were shown in Fig. 5b include: (1) The one-electron transferred from the fluorine atoms toward the copper substrate, forming the interface bonding between fluorine and copper substrate; (2) the induced intermediate radical anion of fluorine were attracted to the dissolved Cu^{2+} ions, leading to the ionic bonding of C–F–Cu–F–C between FG sheets; (3) the FG sheets were dissociated into carbon radicals and fluorine anions due to the high positive bias on the anode. Note that the interface and interlayer bonding as we mentioned in the pathway (1) and (2) could also be formed as carbon radicals and the F^- anions reached the Cu substrate or the Cu^{2+} ions. The remained Cu^{2+} ions and the F^- anions would ionic-bond together and precipitated as CuF_2 crystal particles (TEM in Fig. 4c) among the FG film when the ethanol was evaporated after the EPD process since it was known that the CuF_2 crystal is soluble in ethanol. In the crystal structure of

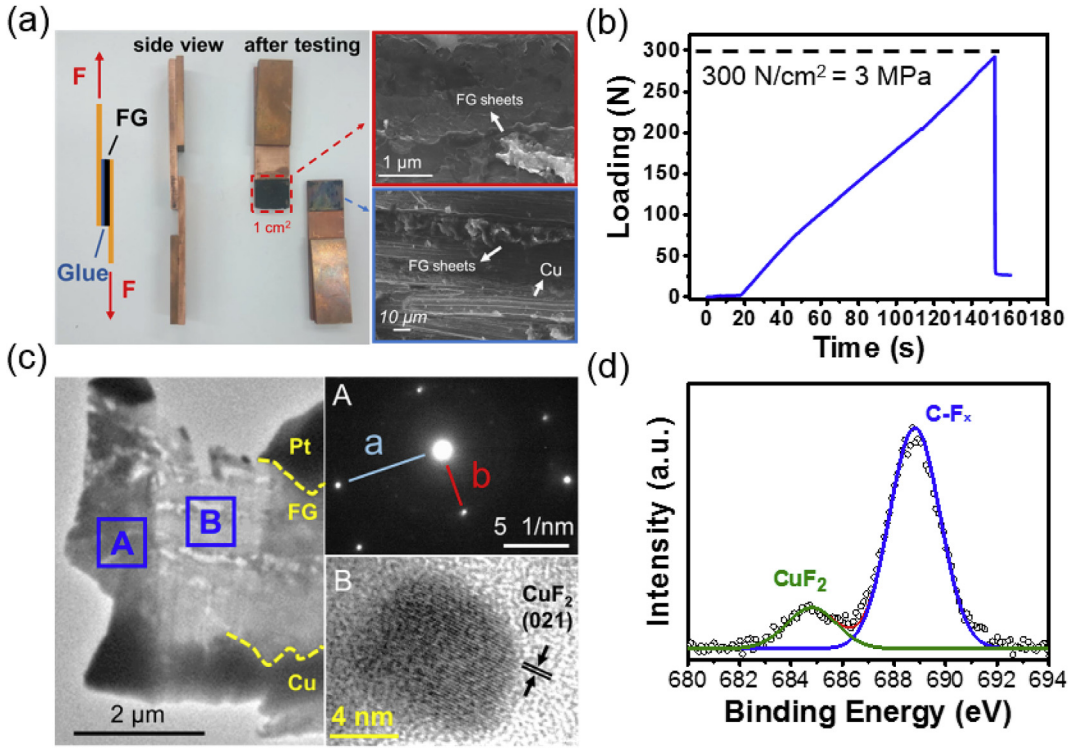

Fig. 4. (a) Optical images of tensile testing samples (left), fracture interface after testing (middle), and SEM image of fracture interface of peeled off FG film (top right) and copper substrate (bottom right). (b) The loading-time curve of tensile testing. (c) HRTEM images of the FG film cross-section (left) and their SAED pattern of region A and higher magnification of region B. (d) F1s XPS of the copper substrate after peeling off the FG film. (A colour version of this figure can be viewed online.)

copper fluoride, each fluorine atoms would bond with 2 copper atoms by ionic bonding. The nature of bonding between Cu and FG would favor to replacing one of the Cu–F in Cu–F–Cu into semi-ionic bonding C–F so as to form the Cu–F–C bond. The interface and the interlayer bonding would be formed with graphene through the covalent C–C bonding, where the semi-ionic C–F bonds link to the ionic Cu–F bonds followed by coupling to a metallic Cu–Cu bonding or another FG sheet (Fig. S9). Therefore, the *in situ*-formed CuF_2 was suggested to result in ultrastrong adhesion between the FG film and the copper substrate.

The corrosion of Cu substrate was unavoidable during the EPD process because of the high applied positive bias. To reduce the corrosion effect on the substrate a short duration of EPD could be employed. For example, for the applied voltage of 50 V for 30 s, a hydrophobic surface could also be obtained (CA = 112.46°) while the initial corrosion could be decreased to 3.6 nm. The alternative method is to lower the applied voltage. Fig. S8 showed the EDP current under different conditions (w/wo FG). When the applied voltage decreased from 50 V to 10 V, the average current was decreased from 310 to 59 μA, indicated a lower corrosion rate. By EPD with 10 V for 10 min, the CA was 110.92° and the corrosion rate was decreased to 0.73 mm/year and the initial corrosion was decreased to 13.7 nm. In this regard, the optimized condition to balance the hydrophobicity and initial corrosion was 10 V for 1 min, from which a higher CA (122.44°) with lower corrosion of mother metal (1.37 nm) can be obtained. In conclusion, there is a trade-off between the corrosion rate of mother substrate and deposition rate of FG. Both of the lower voltage and short duration can suppress the corrosion issue, but the deposition rate and surface uniformity/coverage-rate of FG film was limited.

Moreover, the FG film showed high thermal stability under an ambient atmosphere at a high temperature. Fig. 6a shows the CA evolution of the FG films synthesized at 50 V for 10 min when they were subjected to heating at different temperatures from room temperature to 325 °C in air for 1 h. The increase in the CA at 175 °C and the narrowing of the error bar indicated that the film became more hydrophobic and uniform, which was attributed to the release of the solvent residue; thus, the FG could expose more C–F states on the flake surface. In addition, the contact angle was maintained at approximately 110° when the temperature was below 300 °C, while it decreased abruptly to 76.96° at 325 °C. To understand the evolution of chemical bonding on the FG films when subjected to thermal reaction, XPS measurements were carried out to analyze the chemical bonding of the film with heating treatment at 400 °C (Fig. 6b). The disappearance of CF-CF_2, C–F_2, and C–F_3 bonding indicated the release of fluorine atoms from FG, which reduced the hydrophobicity of the FG film. On the other hand, the FG film also showed good stability when it was exposed to air, as shown in Fig. 6c. The contact angle of the FG film gradually decreased from 112.76° to 106.37° within the first 7 days, which was attributed to the flattened surface of FG when solvent vaporization occurred, resulting in a decrease in the surface energy due to the decrease in physical structure hydrophobicity. The contact angle stabilized at 106.2° for over 28 days, suggesting long-term stability of the material when exposed to ambient conditions. To demonstrate the potential application of the FG and the EPD coating technology, Fig. 6d shows that the FG film prepared by the EPD method can be coated on a brass screw with high uniformity, covering the whole complex surface, indicating the high feasibility and scalability of this process with target substrates of various shapes. In addition, the surface of the FG-coated screw shows much higher hydrophobicity than the pristine screw, even with water drops between the screw threads, further demonstrating the conformal coating on the substrate surface by this method. This

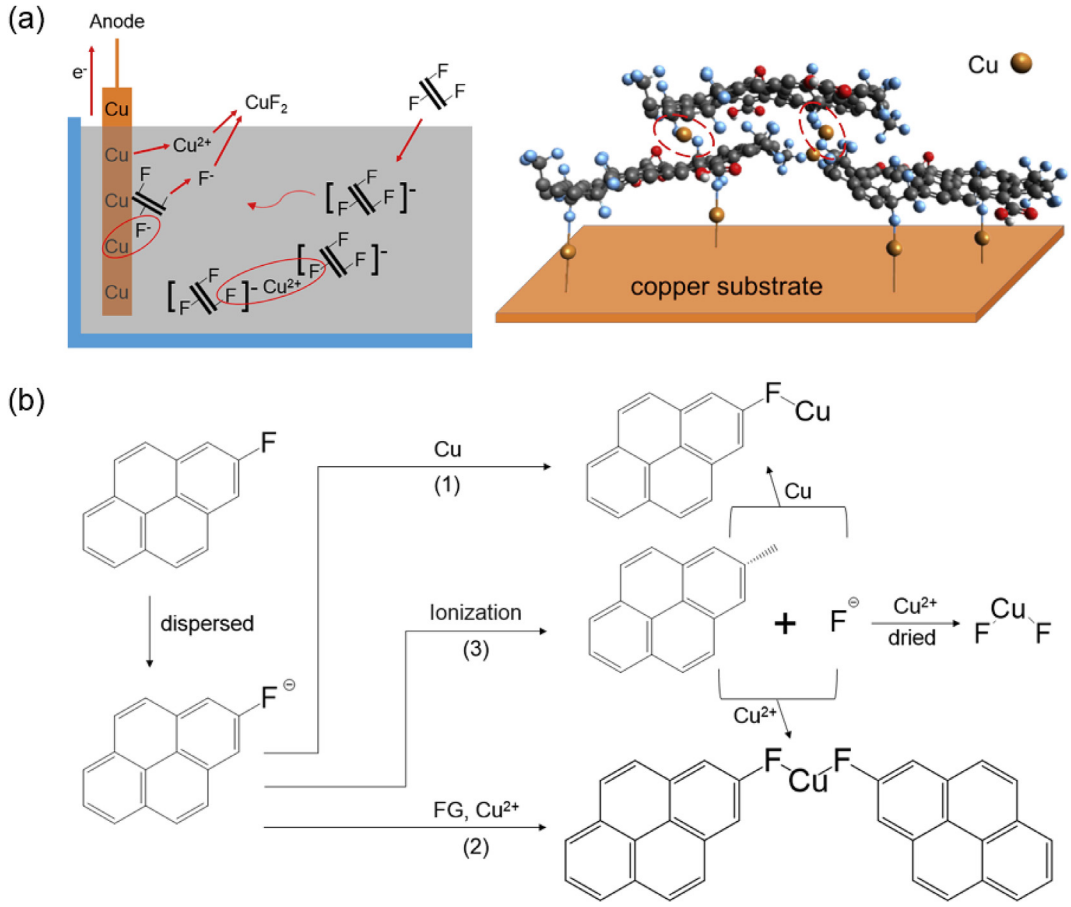

Fig. 5. (a) The in situ formation of the interface and interlayer material models bringing ultrastrong adhesion during the EPD process. (b) The reaction pathways of interface and interlayer bonding formation and the precipitation of copper fluoride particles. (A colour version of this figure can be viewed online.)

EPD method, with its high controllability and high adhesion, serves as a more efficient way to perform hydrophobicity surface modification. It is worth noting that the FG-coated screw in this study demonstrated the unique application of not only the strong adhesion and hydrophobic surface but also the additional properties of extremely low surface friction coefficient [37,63] and thermal stability as well as the anticorrosion [64,65] of FG. Achieving these abovementioned properties of FG could bring a revolutionary breakthrough in terms of functional coatings for versatile applications, including as the key components in more durable aerospace materials and in infrastructure under harsh environments.

4. Conclusion

In this study, FG was successfully synthesized by a simple and scalable hydrothermal process using a mixture of poly(perfluorosulfonic acid) (PFSA) as the precursor in a graphene oxide (GO) solution. Moreover, for the first time, we discovered an unexpected, novel approach to deposit FG on a copper substrate by electrophoretic deposition (EPD), resulting in transformation to ionic-covalent bonded states (Cu-F-C) between FG sheets and the underlying copper due to in situ electrochemical conversion and formation of CuF_2, leading to ultrastrong adhesion at the interface of up to 3 MPa without adding any polymer binders, thus resolving the previously reported issue of low adhesion that normally occurs in graphene and other 2D materials. The hydrophobic surface of the copper was successfully modified by increasing the contact angle from 83.43° to 122.44°. Furthermore, the FG film also showed superior thermal stability up to 300 °C in the ambient atmosphere without loss of hydrophobicity. With the high controllability and high adhesion of the deposited FG film by this method, this study provided a more efficient, feasible and scalable way to achieve surface modification on target substrates of various shapes.

CRediT authorship contribution statement

Yu-Yu Sin: Methodology, Software, Writing - original draft, Investigation. **Cheng-Chun Huang:** Project administration, Data curation. **Cin-Nan Lin:** Methodology, Software, Validation. **Jui-Kung Chih:** Investigation, Data curation. **Yu-Ling Hsieh:** Methodology, Data curation. **I-Yu Tsao:** Visualization, Data curation. **Ju Li:** Investigation, Writing - original draft, preparation. **Ching-Yuan Su:** Conceptualization, Supervision, Writing - review & editing.

Declaration of competing interest

The authors declare that they have no known competing financial interests or personal relationships that could have appeared to influence the work reported in this paper.

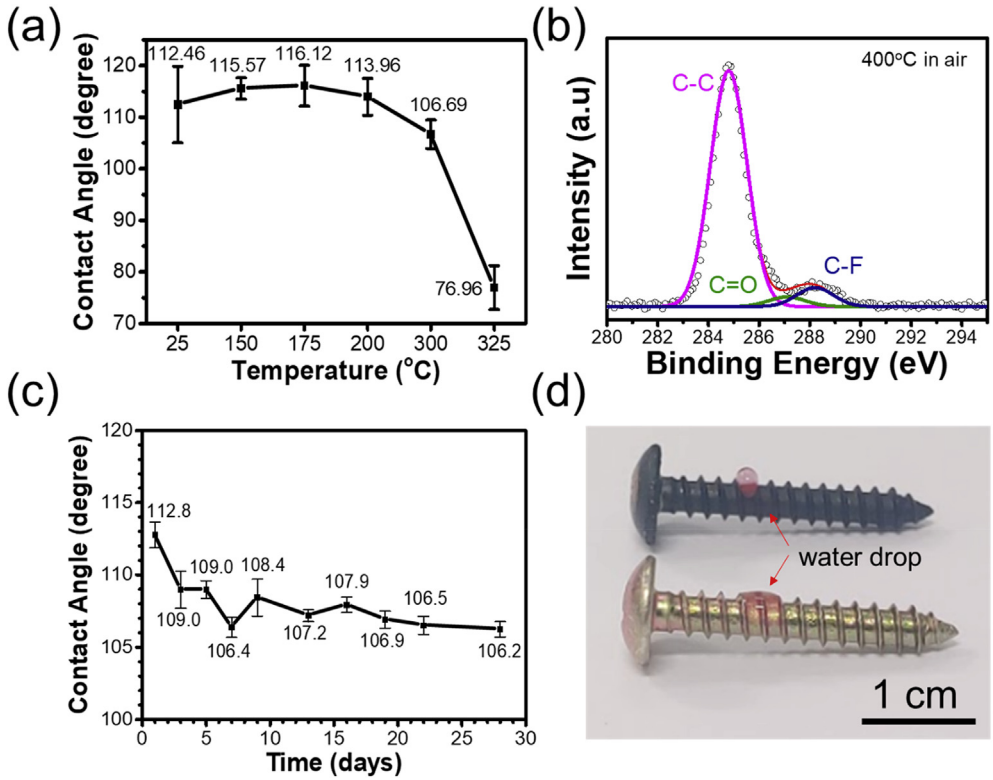

Fig. 6. (a) Contact angle of the 50 V/30 s FG film after heating at different temperatures and (b) C1s XPS after heating at 400 °C. (c) The contact angle of the 50 V/30 s FG film after placement at room temperature and pressure for up to 28 days. (d) FG film deposited on the complex surface of a brass screw by the EPD process. The water drop (with red dye) demonstrated a more hydrophobic surface than that of the pristine screw. (A colour version of this figure can be viewed online.)

Acknowledgements

This research was supported by the Ministry of Science and Technology, Taiwan under grants number of 109-2628-E-008 -002 -MY3, 108-3116-F-008-005 and 106-2221-E-008-087-MY3. The authors acknowledge the technical services provided by the Precision Instrument Center of National Central University.

Appendix A. Supplementary data

Supplementary data to this article can be found online at https://doi.org/10.1016/j.carbon.2020.07.067.

Declaration of AFMRC project

This paper is not based on AFMRC Project.

References

[1] Y. Wang, J. Xue, Q. Wang, Q. Chen, J. Ding, Verification of icephobic/anti-icing properties of a superhydrophobic surface, ACS Appl. Mater. Interfaces 5 (8) (2013) 3370–3381.
[2] E. Schmidt, W. Schurig, W. Sellschopp, Versuche über die Kondensation von Wasserdampf in Film-und Tropfenform, Technische Mechanik und Thermodynamik 1 (2) (1930) 53–63.
[3] X.-M. Li, D. Reinhoudt, M. Crego-Calama, What do we need for a superhydrophobic surface? A review on the recent progress in the preparation of superhydrophobic surfaces, Chem. Soc. Rev. 36 (8) (2007) 1350–1368.
[4] J. Rose, Dropwise condensation theory and experiment: a review, Proc. IME J. Power Energy 216 (2) (2002) 115–128.
[5] D.J. Preston, D.L. Mafra, N. Miljkovic, J. Kong, E.N. Wang, Scalable graphene coatings for enhanced condensation heat transfer, Nano Lett. 15 (5) (2015) 2902–2909.
[6] Y.Y. Yan, N. Gao, W. Barthlott, Mimicking natural superhydrophobic surfaces and grasping the wetting process: a review on recent progress in preparing superhydrophobic surfaces, Adv. Colloid Interface Sci. 169 (2) (2011) 80–105.
[7] C. Parra, F. Dorta, E. Jimenez, R. Henríquez, C. Ramírez, R. Rojas, P. Villalobos, A nanomolecular approach to decrease adhesion of biofouling-producing bacteria to graphene-coated material, J. Nanobiotechnol. 13 (1) (2015) 82.
[8] X. Li, W. Cai, J. An, S. Kim, J. Nah, D. Yang, R. Piner, A. Velamakanni, I. Jung, E. Tutuc, Large-area synthesis of high-quality and uniform graphene films on copper foils, Science 324 (5932) (2009) 1312–1314.
[9] X. Li, G. Zhang, X. Bai, X. Sun, X. Wang, E. Wang, H. Dai, Highly conducting graphene sheets and Langmuir–Blodgett films, Nat. Nanotechnol. 3 (9) (2008) 538.
[10] F. Torrisi, T. Hasan, W. Wu, Z. Sun, A. Lombardo, T.S. Kulmala, G.-W. Hsieh, S. Jung, F. Bonaccorso, P.J. Paul, Inkjet-printed graphene electronics, ACS Nano 6 (4) (2012) 2992–3006.
[11] S. Das, D. Lahiri, D.-Y. Lee, A. Agarwal, W. Choi, Measurements of the adhesion energy of graphene to metallic substrates, Carbon 59 (2013) 121–129.
[12] T. Yoon, W.C. Shin, T.Y. Kim, J.H. Mun, T.-S. Kim, B.J. Cho, Direct measurement of adhesion energy of monolayer graphene as-grown on copper and its application to renewable transfer process, Nano Lett. 12 (3) (2012) 1448–1452.
[13] Y.Q. Li, T. Yu, T.Y. Yang, L.X. Zheng, K. Liao, Bio-inspired nacre-like composite films based on graphene with superior mechanical, electrical, and biocompatible properties, Adv. Mater. 24 (25) (2012) 3426–3431.
[14] K.W. Putz, O.C. Compton, M.J. Palmeri, S.T. Nguyen, L.C. Brinson, High-nanofiller-content graphene oxide–polymer nanocomposites via vacuum-assisted self-assembly, Adv. Funct. Mater. 20 (19) (2010) 3322–3329.
[15] Y. Gao, L.-Q. Liu, S.-Z. Zu, K. Peng, D. Zhou, B.-H. Han, Z. Zhang, The effect of interlayer adhesion on the mechanical behaviors of macroscopic graphene oxide papers, ACS Nano 5 (3) (2011) 2134–2141.
[16] P. Flouda, S.A. Shah, D.C. Lagoudas, M.J. Green, J.L. Lutkenhaus, Highly multifunctional dopamine-functionalized reduced graphene oxide supercapacitors, Matter 1 (6) (2019) 1532–1546.
[17] W. Cui, M. Li, J. Liu, B. Wang, C. Zhang, L. Jiang, Q. Cheng, A strong integrated strength and toughness artificial nacre based on dopamine cross-linked graphene oxide, ACS Nano 8 (9) (2014) 9511–9517.
[18] Y. Liu, C. Liang, A. Wei, Y. Jiang, Q. Tian, Y. Wu, Z. Xu, Y. Li, F. Guo, Q. Yang, Solder-free electrical Joule welding of macroscopic graphene assemblies, Mater. Today Nano 3 (2018) 1–8.
[19] H. Xu, J. Zang, Y. Yuan, P. Tian, Y. Wang, Preparation of multilayer graphene coatings with interfacial bond to mild steel via covalent bonding for high performance anticorrosion and wear resistance, Carbon 154 (2019) 156–168.
[20] V. Sreepal, M. Yagmurcukardes, K.S. Vasu, D.J. Kelly, S.F.R. Taylor, V.G. Kravets, Z. Kudrynskyi, Z.D. Kovalyuk, A. Patanè, A.N. Grigorenko, Two-dimensional

covalent crystals by chemical conversion of thin van der Waals materials, Nano Lett. 19 (9) (2019) 6475–6481.
[21] L.A. Chernozatonskii, P.B. Sorokin, A.G.e. Kvashnin, D.G.e. Kvashnin, Diamond-like C 2 H nanolayer, diamane: simulation of the structure and properties, JETP Lett. (Engl. Transl.) 90 (2) (2009) 134–138.
[22] M.A. Ribas, A.K. Singh, P.B. Sorokin, B.I. Yakobson, Patterning nanoroads and quantum dots on fluorinated graphene, Nano Res. 4 (1) (2011) 143–152.
[23] A.P. Barboza, M.H. Guimaraes, D.V. Massote, L.C. Campos, N.M. Barbosa Neto, L.G. Cancado, R.G. Lacerda, H. Chacham, M.S. Mazzoni, B.R. Neves, Room-temperature compression-induced diamondization of few-layer graphene, Adv. Mater. 23 (27) (2011) 3014–3017.
[24] D. Odkhuu, D. Shin, R.S. Ruoff, N. Park, Conversion of multilayer graphene into continuous ultrathin sp 3-bonded carbon films on metal surfaces, Sci. Rep. 3 (2013) 3276.
[25] A.G. Kvashnin, L.A. Chernozatonskii, B.I. Yakobson, P.B. Sorokin, Phase diagram of quasi-two-dimensional carbon, from graphene to diamond, Nano Lett. 14 (2) (2014) 676–681.
[26] P.V. Bakharev, M. Huang, M. Saxena, S.W. Lee, S.H. Joo, S.O. Park, J. Dong, D.C. Camacho-Mojica, S. Jin, Y. Kwon, Chemically induced transformation of chemical vapour deposition grown bilayer graphene into fluorinated single-layer diamond, Nat. Nanotechnol. 15 (1) (2020) 59–66.
[27] Y. Gao, T. Cao, F. Cellini, C. Berger, W.A. De Heer, E. Tosatti, E. Riedo, A. Bongiorno, Ultrahard carbon film from epitaxial two-layer graphene, Nat. Nanotechnol. 13 (2) (2018) 133–138.
[28] L.G.P. Martins, M.J. Matos, A.R. Paschoal, P.T. Freire, N.F. Andrade, A.L. Aguiar, J. Kong, B.R. Neves, A.B. de Oliveira, M.S. Mazzoni, Raman evidence for pressure-induced formation of diamondene, Nat. Commun. 8 (1) (2017) 1–9.
[29] M. Diba, D.W. Fam, A.R. Boccaccini, M.S. Shaffer, Electrophoretic deposition of graphene-related materials: a review of the fundamentals, Prog. Mater. Sci. 82 (2016) 83–117.
[30] S. Kim, J.-S. Oh, M.-G. Kim, W. Jang, M. Wang, Y. Kim, H.W. Seo, Y.C. Kim, J.-H. Lee, Y. Lee, Electromagnetic interference (EMI) transparent shielding of reduced graphene oxide (RGO) interleaved structure fabricated by electrophoretic deposition, ACS Appl. Mater. Interfaces 6 (20) (2014) 17647–17653.
[31] X. Jiang, Y. Cao, K. Wang, J. Wei, D. Wu, H. Zhu, Anti-reflection graphene coating on metal surface, Surf. Coating. Technol. 261 (2015) 327–330.
[32] J.H. Park, J.M. Park, Electrophoretic deposition of graphene oxide on mild carbon steel for anti-corrosion application, Surf. Coating. Technol. 254 (2014) 167–174.
[33] W. He, L. Zhu, H. Chen, H. Nan, W. Li, H. Liu, Y. Wang, Electrophoretic deposition of graphene oxide as a corrosion inhibitor for sintered NdFeB, Appl. Surf. Sci. 279 (2013) 416–423.
[34] J.T. Robinson, J.S. Burgess, C.E. Junkermeier, S.C. Badescu, T.L. Reinecke, F.K. Perkins, M.K. Zalalutdniov, J.W. Baldwin, J.C. Culbertson, P.E. Sheehan, Properties of fluorinated graphene films, Nano Lett. 10 (8) (2010) 3001–3005.
[35] W. Feng, P. Long, Y. Feng, Y. Li, Two-dimensional fluorinated graphene: synthesis, structures, properties and applications, Adv. Sci. 3 (7) (2016) 1500413.
[36] V. Wheeler, N. Garces, L. Nyakiti, R. Myers-Ward, G. Jernigan, J. Culbertson, C. Eddy Jr., D.K. Gaskill, Fluorine functionalization of epitaxial graphene for uniform deposition of thin high-κ dielectrics, Carbon 50 (6) (2012) 2307–2314.
[37] S. Kwon, J.-H. Ko, K.-J. Jeon, Y.-H. Kim, J.Y. Park, Enhanced nanoscale friction on fluorinated graphene, Nano Lett. 12 (12) (2012) 6043–6048.
[38] K.I. Ho, J.H. Liao, C.H. Huang, C.L. Hsu, W. Zhang, A.Y. Lu, L.J. Li, C.S. Lai, C.Y. Su, One-Step formation of a single atomic-layer transistor by the selective fluorination of a graphene film, Small 10 (5) (2014) 989–997.
[39] K.-I. Ho, C.-H. Huang, J.-H. Liao, W. Zhang, L.-J. Li, C.-S. Lai, C.-Y. Su, Fluorinated graphene as high performance dielectric materials and the applications for graphene nanoelectronics, Sci. Rep. 4 (2014) 5893.
[40] D.D. Chronopoulos, A. Bakandritsos, M. Pykal, R. Zbořil, M. Otyepka, Chemistry, properties, and applications of fluorographene, Appl. Mater. Today 9 (2017) 60–70.
[41] C.-Y. Su, C.-Y. Yang, B.-W. Jhang, Y.-L. Hsieh, Y.-Y. Sin, C.-C. Huang, Pool boiling heat transfer enhanced by fluorinated graphene as atomic layered modifiers, ACS Appl. Mater. Interfaces 12 (9) (2020) 10233–10239.
[42] A. Mathkar, T. Narayanan, L.B. Alemany, P. Cox, P. Nguyen, G. Gao, P. Chang, R. Romero-Aburto, S.A. Mani, P. Ajayan, Synthesis of fluorinated graphene oxide and its amphiphobic properties, Part. Part. Syst. Char. 30 (3) (2013) 266–272.
[43] A. Tuteja, W. Choi, M. Ma, J.M. Mabry, S.A. Mazzella, G.C. Rutledge, G.H. McKinley, R.E. Cohen, Designing superoleophobic surfaces, Science 318 (5856) (2007) 1618–1622.
[44] R.R. Nair, W. Ren, R. Jalil, I. Riaz, V.G. Kravets, L. Britnell, P. Blake, F. Schedin, A.S. Mayorov, S. Yuan, Fluorographene: a two-dimensional counterpart of Teflon, Small 6 (24) (2010) 2877–2884.
[45] L. Bulusheva, V. Tur, E. Fedorovskaya, I. Asanov, D. Pontiroli, M. Riccò, A. Okotrub, Structure and supercapacitor performance of graphene materials obtained from brominated and fluorinated graphites, Carbon 78 (2014) 137–146.
[46] O. Jankovský, V. Mazánek, K. Klímová, D. Sedmidubský, J. Kosina, M. Pumera, Z. Sofer, Simple synthesis of fluorinated graphene: thermal exfoliation of fluorographite, Chem.–A Eur. J. 22 (49) (2016) 17696–17703.
[47] Z. Wang, J. Wang, Z. Li, P. Gong, X. Liu, L. Zhang, J. Ren, H. Wang, S. Yang, Synthesis of fluorinated graphene with tunable degree of fluorination, Carbon 50 (15) (2012) 5403–5410.
[48] K. Samanta, S. Some, Y. Kim, Y. Yoon, M. Min, S.M. Lee, Y. Park, H. Lee, Highly hydrophilic and insulating fluorinated reduced graphene oxide, Chem. Commun. 49 (79) (2013) 8991–8993.
[49] C.-Y. Su, Y. Xu, W. Zhang, J. Zhao, X. Tang, C.-H. Tsai, L.-J. Li, Electrical and spectroscopic characterizations of ultra-large reduced graphene oxide monolayers, Chem. Mater. 21 (23) (2009) 5674–5680.
[50] C.-Y. Su, Y. Xu, W. Zhang, J. Zhao, A. Liu, X. Tang, C.-H. Tsai, Y. Huang, L.-J. Li, Highly efficient restoration of graphitic structure in graphene oxide using alcohol vapors, ACS Nano 4 (9) (2010) 5285–5292.
[51] S. Radhakrishnan, D. Das, A. Samanta, A. Carlos, L. Deng, L.B. Alemany, T.K. Weldeghiorghis, V.N. Khabashesku, V. Kochat, Z. Jin, Fluorinated h-BN as a magnetic semiconductor, Sci. Adv. 3 (7) (2017) e1700842.
[52] M. Feng, R. Qu, Z. Wei, L. Wang, P. Sun, Z. Wang, Characterization of the thermolysis products of Nafion membrane: a potential source of perfluorinated compounds in the environment, Sci. Rep. 5 (2015) 9859.
[53] K. Krishnamoorthy, M. Veerapandian, K. Yun, S.-J. Kim, The chemical and structural analysis of graphene oxide with different degrees of oxidation, Carbon 53 (2013) 38–49.
[54] D.K. Samarakoon, Z. Chen, C. Nicolas, X.Q. Wang, Structural and electronic properties of fluorographene, Small 7 (7) (2011) 965–969.
[55] K.-I. Ho, J.-H. Liao, C.-H. Huang, C.-L. Hsu, L.-J. Li, C.-S. Lai, C.-Y. Su, One-step formation of atomic-layered transistor by selective fluorination of graphene film, in: 2013 IEEE 5th International Nanoelectronics Conference (INEC), IEEE, 2013, pp. 326–328.
[56] K.-I. Ho, J.-H. Liao, C.-H. Huang, C.-L. Hsu, W. Zhang, A.-Y. Lu, L.-J. Li, C.-S. Lai, C.-Y. Su, One-Step formation of a single atomic-layer transistor by the selective fluorination of a graphene film, Small 10 (5) (2014) 989–997.
[57] Y.C. Wang, I.C. Leu, M.H. Hon, Kinetics of electrophoretic deposition for nanocrystalline zinc oxide coatings, J. Am. Ceram. Soc. 87 (1) (2004) 84–88.
[58] I. Zhitomirsky, L. Gal-Or, Electrophoretic deposition of hydroxyapatite, J. Mater. Sci. Mater. Med. 8 (4) (1997) 213–219.
[59] S. Yang, L. Chen, C. Wang, M. Rana, P.-C. Ma, Surface roughness induced superhydrophobicity of graphene foam for oil-water separation, J. Colloid Interface Sci. 508 (2017) 254–262.
[60] J.E. Andrews, Y. Wang, S. Sinha, P.W. Chung, S. Das, Roughness-induced chemical heterogeneity leads to large hydrophobicity in wetting-translucent nanostructures, J. Phys. Chem. C 121 (18) (2017) 10010–10017.
[61] F. Badway, A. Mansour, N. Pereira, J. Al-Sharab, F. Cosandey, I. Plitz, G. Amatucci, Structure and electrochemistry of copper fluoride nanocomposites utilizing mixed conducting matrices, Chem. Mater. 19 (17) (2007) 4129–4141.
[62] W.W. Liu, J.N. Wang, X.X. Wang, Charging of unfunctionalized graphene in organic solvents, Nanoscale 4 (2) (2012) 425–428.
[63] D. Petrova, B. Weber, C. Allain, P. Audebert, C.H. Venner, A.M. Brouwer, D. Bonn, Fluorescence microscopy visualization of the roughness-induced transition between lubrication regimes, Sci. Adv. 5 (12) (2019) eaaw4761.
[64] Z. Yang, W. Sun, L. Wang, S. Li, T. Zhu, G. Liu, Liquid-phase exfoliated fluorographene as a two dimensional coating filler for enhanced corrosion protection performance, Corrosion Sci. 103 (2016) 312–318.
[65] Z. Yang, L. Wang, W. Sun, S. Li, T. Zhu, W. Liu, G. Liu, Superhydrophobic epoxy coating modified by fluorographene used for anti-corrosion and self-cleaning, Appl. Surf. Sci. 401 (2017) 146–155.